Polymer Chemistry

Poly(para-phenylene) ionomer membranes: effect of methyl and trifluoromethyl substituents

Journal:	*Polymer Chemistry*
Manuscript ID	PY-ART-08-2021-001141.R1
Article Type:	Paper
Date Submitted by the Author:	10-Sep-2021
Complete List of Authors:	Liu, Fanghua; University of Yamanashi, Clean Energy Research Ann, Jinju; KIER, Miyake, Junpei; University of Yamanashi, Miyatake, Kenji; University of Yamanashi, Clean Energy Research

ARTICLE

Poly(*para*-phenylene) ionomer membranes: effect of methyl and trifluoromethyl substituents

Received 00th January 20xx,
Accepted 00th January 20xx

DOI: 10.1039/x0xx00000x

Fanghua Liu[a], Jinju Ahn[b], Junpei Miyake[c] and Kenji Miyatake*[,c,d,e]

Sulfonated poly(*para*-phenylene)s with high molecular weight and membrane forming capability were obtained by use of the effect of methyl and trifluoromethyl substituents. The linearity of the polymer main chain decreased by introducing these substituents; persistence length (l_p, index of linearity, distance required for a polymer chain to bend by 90° on average) of homopolymers for 2,2'-dimethyl-1,1'-biphenyl (BP-CH_3), 2,2'-bis(trifluoromethyl)-1,1'-biphenyl (BP-CF_3) were ca. 350.6 nm and 87.7 nm, respectively, estimated by numerically averaging backbone conformations. Copolymers with sulfo-*para*-phenylene, SPP-BP-CH_3 and -CF_3, were obtained as high molecular weight (M_n = 28 – 30 kDa, M_w = 88 – 100 kDa for SPP-BP-CH_3 and M_n = 49 – 149 kDa, M_w = 161 – 316 kDa for SPP-BP-CF_3, respectively) to provide flexible membranes by casting from the solution. Despite more hydrophobic nature of the substituents, SPP-BP-CF_3 membranes showed higher water uptake and proton conductivity than those of SPP-BP-CH_3 membranes with comparable ion exchange capacity (IEC). SPP-BP-CF_3 membranes showed slightly higher maximum strain (2.9-5.2%) than that (1.1-2.1%) of SPP-BP-CH_3 membranes leading to the higher rapture energy as expected from the smaller persistence length of the BP-CF_3 homopolymers. While SPP-BP-CH_3 decomposed under the harsh oxidative conditions, SPP-BP-CF_3 were more oxidatively stable and exhibited negligible changes in weight, molecular weight, molecular structure and membrane properties (proton conductivity, mechanical properties etc).

Introduction

Poly(*para*-phenylene) is one of the simplest synthetic polymers composed solely of *para*-linked phenylene groups. Because of the linear and rigid main chain structure, poly(*para*-phenylene) has very low solvent solubility causing difficulty in obtaining high-molecular-weight polymers.[1-6] To increase the solvent solubility and molecular weight of poly(*para*-phenylene), introducing functional groups (i.e., substituted poly(*para*-phenylene)s) is an effective and promising approach.[7-11] The effects of functional groups are mainly classified into three aspects; increasing of conformational entropy, alterations of polymer main chain conformation, and provoking of additional functions. For example, bulky substituents increased the conformational entropy generated by the large number of conformational isomers of the side groups.[12] This provided poly(*para*-phenylene)s with solvent solubility, which enabled the formation of high-molecular-weight poly(*para*-phenylene)s (e.g., the obtainable soluble fragments for substituted poly(*para*-phenylene)s had much higher degree of polymerization (DP) of 101 (M_n = 20,030 Da) than that (DP ≤ 6) for unsubstituted poly(*para*-phenylene)s).[13] Regarding the polymer main chain conformation, the linearity of poly(*para*-phenylene)s decreases with increasing the bulkiness of substituents due to the steric hindrance. Vaia et al. reported that benzoyl-substituted poly(*para*-phenylene)s had the persistence length (l_p)[14] which was far smaller (or more bent structure) than that (l_p of infinity) for unsubstituted poly(*para*-phenylene) on the assumption of 180° bond angle for *para*-phenylene linkage. The resulting benzoyl-substituted poly(*para*-phenylene)s were amorphous and showed traditional thermoplastic viscoelastic properties in the solid state and melt (glass transition temperature of 206 °C).[15] Small persistence length seemed to bring about polymer chain entanglement and eventually membrane forming capability.

The excellent thermal, hydrolytic and oxidative stabilities intrinsic to poly(*para*-phenylene)s are attractive as ion conductive polymers,[16-19] in particular, for the application to energy devices such as fuel cells. Acid-functionalization provides poly(*para*-phenylene)s with proton conductive properties. Recently, Holdcroft et al. found that sulfonated phenylated polyphenylene derivatives including biphenyl linked SPPB-H^+ and naphthalene linked SPPN-H^+ formed thin membranes. The membranes functioned well as proton exchange membrane for fuel cells, exhibiting high proton conductivity (268 and 172 mS cm^{-1} under 95% RH and 80 °C for SPPN-H^+ and SPPB-H^+, respectively), oxidative stability (0.09

[a] *Graduate School of Medical, Industrial and Agricultural Science, University of Yamanashi, Kofu, Yamanashi 400-8510, Japan.*
[b] *Interdisciplinary Graduate School of Medicine and Engineering, University of Yamanashi, Kofu, Yamanashi 400-8510, Japan.*
[c] *Clean Energy Research Center, University of Yamanashi, Kofu, Yamanashi 400-8510, Japan.*
[d] *Fuel Cell Nanomaterials Center, University of Yamanashi, Kofu, Yamanashi 400-8510, Japan.*
[e] *Department of Applied Chemistry, and Research Institute for Science and Engineering, Waseda University, Tokyo 169-8555, Japan.*
† Electronic Supplementary Information (ESI) available. See DOI: 10.1039/x0xx00000x

±0.62% and 0.69 ± 0.71% mass loss after Fenton's test at 80 °C for 1 h for SPPN-H^+ and SPPB-H^+, respectively) and fuel cell performance (power density of 927 and 1237 mW·cm^{-2} at 80 °C, no backpressure under RH cycling (90-100% RH at the cathode and 95-100% RH at the anode) for SPPN-H^+ and SPPB-H^+, respectively).[20] More recently, it was reported that the composition of polyphenylene backbone (i.e. the ratio among *ortho*-, *meta*- and *para*-phenylene groups) had a great impact on the bulk properties.[21-23] By precisely controlling the ratio of *meta*-/*para*-phenylene (4:1) groups, we successfully developed simpler sulfonated poly(phenylene)s with no other substituents having flexible membrane forming capability. The sulfonated polyphenylene-based membrane (SPP-QP) exhibited excellent chemical stability (1% mass loss after immersing the membrane in Fenton's reagent at 80 °C for 1 h) and reasonable mechanical properties (elongation at break = 68% at 80 °C and 60% RH).[24] To the best of our knowledge, there have been only limited reports focusing on sulfonated poly(*para*-phenylene)s (containing no *ortho*- and *meta*-phenylene groups) without any vulnerable heteroatom linkages that exhibited high membrane formability available as proton exchange membranes. Litt et al. synthesized water-soluble and low molecular weight poly(*para*-phenylene disulfonic acid) (PPDSA and PBPDSA) by Ullmann reaction.[25] By modifying (grafting of alkylbenzene groups), a series of grafted copolymers still exhibited excess water absorbability. The mechanical properties and chemical stability were not evaluated.[26] Herein we report, thin membranes high molecular weight from methyl or trifluoromethyl substituted, sulfonated poly(*para*-phenylene)s. Effect of those substituents on synthesis, structure, and membrane properties of the sulfonated poly(*para*-phenylene)s was investigated in detail.

Experiments

Materials. 2,5-Dichlorobenzenesulfonic acid dihydrate (SP) (TCI), *m*-toluidine (TCI), 2,2'-bis(trifluoromethyl)benzidine (TCI), bis(1,5-cyclooctadiene)nickel(0) ($Ni(COD)_2$) (> 95%, Kanto Chemical), 2,2'-bipyridine (> 99%, Kanto Chemical), copper (I) chloride (> 99%, Kanto Chemical), sodium nitrite (Kanto Chemical), potassium carbonate (Kanto Chemical), sodium chloride (Kanto Chemical), dimethyl sulfoxide (DMSO) (> 99%, Kanto Chemical), and toluene (> 99%, Kanto Chemical) were used as received. Other chemicals were of commercially available grade and used as received.

Synthesis of 4,4'-dichloro-2,2'-bis(methyl)biphenyl (BP-CH_3). In a 1 L round bottomed flask, *m*-toluidine (2.50 g, 11.78 mmol), deionized water (70.0 mL) and 12 M hydrochloric acid (45.0 mL) were charged with a magnetic stirring bar. After dissolution, a solution of $NaNO_2$ (2.04 g, 29.56 mmol) in deionized water (7.0 mL) was added slowly into the mixture at 5 °C. Then, a solution of CuCl (4.20 g, 42.42 mmol) in 12 M hydrochloric acid (33.0 mL) was added dropwise into the mixture. After stirring for 24 h at r.t., the mixture was poured into excess of ethyl acetate. The organic layer was washed with 3 M hydrochloric acid and deionized water successively and evaporated. The crude product was purified with silica gel column chromatograph (eluent: hexane) to obtain BP-CH_3 as a white crystalline power in 36% yield (1.06 g, 4.22 mmol).

Synthesis of 4,4'-dichloro-2,2'-bis(trifluoromethyl)biphenyl (BP-CF_3). In a 300 mL round bottomed flask, 2,2'-bis(trifluoromethyl)benzidine (2.00 g, 6.25 mmol) was dissolved in 5 M hydrochloric acid (25.0 mL). To the solution, a mixture of $NaNO_2$ (1.04 g, 15.07 mmol) dissolved in deionized water (3.3 mL) and CuCl (2.22 g, 22.42 mmol) dissolved in 12 M hydrochloric acid (17.0 mL) was added at 5 °C. After stirring for 24 h at r.t., the mixture was poured into excess of ethyl acetate. The organic layer was washed with 3 M hydrochloric acid and deionized water several times and then evaporated. The crude product was purified with short-column chromatography with alumina (eluent: hexane) to obtain BP-CF_3 as a white crystalline powder in 52% yield (1.17 g, 3.26 mmol).

Synthesis of SPP-BP-CH_3. A typical procedure (for target IEC = 3.5 mequiv. g^{-1}) is as follows. BP-CH_3 (0.38 g, 1.51 mmol), SP (0.55 g, 2.09 mmol), K_2CO_3 (0.35 g, 2.53 mmol), 2,2'-bipyridine (2.37 g, 15.17 mmol), DMSO (11.0 mL) and toluene (11.0 mL) were charged into a 100 mL three-neck flask equipped with a Dean Stark trap and nitrogen inlet and outlet. After stirring at 160 °C for 2 h for azeotropic dehydration, the mixture was cooled to 80 °C. Then, $Ni(COD)_2$ (2.08 g, 7.56 mmol) was added to the mixture and the reaction was continued for 3 h. The mixture was poured into large excess of 6 M hydrochloric acid to precipitate a crude product, which was washed with concentrated hydrochloric acid and deionized water several times. After drying in vacuum oven for 12 h, SPP-BP-CH_3 was obtained in 97% yield.

Synthesis of SPP-BP-CF_3. A typical procedure (for target IEC = 3.5 mequiv. g^{-1}) is as follows. BP-CF_3 (0.32 g, 0.90 mmol), SP (0.53 g, 2.00 mmol), K_2CO_3 (0.33 g, 2.40 mmol), 2,2'-bipyridine (1.91 g, 12.19 mmol), DMSO (8.7 mL) and toluene (8.7 mL) were charged into a 100 mL three-neck flask equipped with a Dean Stark trap and nitrogen inlet and outlet. After stirring at 160 °C for 2 h for azeotropic dehydration, the mixture was cooled to 80 °C. Then, $Ni(COD)_2$ (1.68 g, 6.10 mmol) was added to the mixture and the reaction was continued for 3 h. The mixture was poured into large excess of 6 M hydrochloric acid to precipitate a crude product, which was washed with concentrated hydrochloric acid and deionized water several times. After drying in vacuum oven for 12 h, SPP-BP-CF_3 was obtained in 95% yield.

Membrane Preparation. SPP-BP-CH_3 or SPP-BP-CF_3 copolymer was dissolved in DMSO (2-5% w/v). The solution was cast onto a clean, flat glass plate and dried at 80 °C for 12 h. The resulting membranes (ca. 50 μm thick) were converted to acid form by treating with 1 M sulfuric acid for 1 d at r.t., washed with deionized water several times, and dried at 80 °C.

Results and discussions

Molecular design

First, we estimated the effect of methyl (CH_3) and trifluoromethyl (CF_3) substituents on the linearity of poly(*para*-phenylene) chains. It is recognized that poly(*para*-phenylene) (without any substituents) contains linear main chains (i.e., backbone deflection angle of 0°) (Fig. 1(a)). As a quantitative description for backbone flexibility, persistence length (l_p), which expresses the distance required for a polymer backbone to bend by 90° on average;[27] i.e., the higher l_p is, the smaller flexibility the polymer has.[28,29] Previously, Zhang et al. reported that l_p of semiflexible conjugated polymers (for example, poly(3-hexylthiophene)) could be reasonably calculated.[30] Based on the method, we have demonstrated in poly(*meta*-/*para*-phenylene)s (without substituents) that introducing *meta*-phenylene significantly reduced the l_p; it was infinity for 0% *meta*-, 2.67 nm for 20% *meta*-, 1.07 nm for 50% *meta*-, 0.66 nm for 80% *meta*-, and 0.54 nm for 100% *meta*-, respectively.[24]

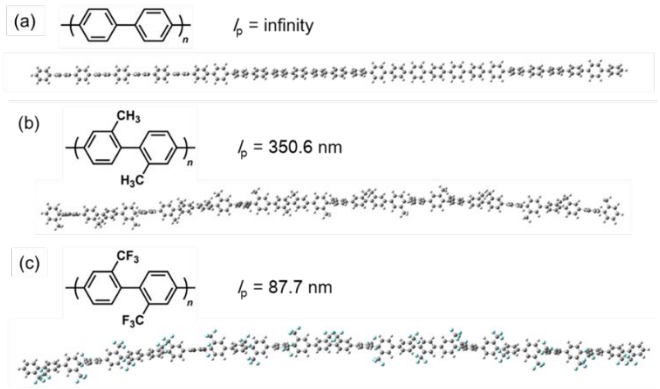

Fig. 1 The optimized 3D structures of (a) BP-H, (b) BP-CH_3 and (c) BP-CF_3 homopolymers. The geometry optimization was conducted for polymers having 30 phenylene rings, by Conflex with MMFF94s force field. The l_p was calculated by numerically averaging 100,000 backbone conformations over a set of suitably generated random dihedral angles (at 300 K, Mathematica).

Similar calculation was applied for the CH_3- and CF_3-substituted poly(*para*-phenylene)s as models for sulfonated SPP-BP-CH_3 and -CF_3. Molecular geometries of the model compounds (i.e., biphenyl (BP-H), 2,2'-dimethyl-1,1'-biphenyl (BP-CH_3), 2,2'-bis(trifluoromethyl)-1,1'-biphenyl (BP-CF_3)) were first determined from structural minimizations, in which the density functional theory (DFT) Becke three-parameter Lee-Yang-Parr (B3LYP) method with 6-311G(2d,p) basis set was used (gas phase, Gaussian09).[24] The backbone deflection angles were dependent on the substituents, and ca. 0° for BP-H, ca. 2° for BP-CH_3, and 4° for BP-CF_3, respectively. Based on these molecular geometries, three kinds of poly(*para*-phenylene) chains (homopolymers of BP-H, BP-CH_3, and BP-CF_3) were created (Fig. 1(a-c)) and their l_p values were calculated by numerically averaging 100,000 backbone conformations over a set of suitably generated random dihedral angles (at 300 K, Mathematica). Note that only the Ph-Ph linkages with *ortho*-hydrogens were rotated and with *ortho*-CH_3 or -CF_3 were not rotated because of much larger rotational barriers of the BP-CH_3 and BP-CF_3 than that of BP-H. The l_p decreased in the order of infinity for BP-H (Fig. 1a), ca. 350.6 nm for BP-CH_3 (Fig. 1b), and 87.7 nm for BP-CF_3 (Fig. 1c). These values seem qualitatively in good agreement with the optimized 3D structures (force field: MMFF94s, Conflex) as shown in Fig. 1. In general, polymer chains with lower l_p are more likely to have membrane-forming capability because of the higher probability of polymer chains entanglement. The simulation results implied possibility of poly(*para*-phenylene) membranes by introducing those simple substituents.

Polymer synthesis

Based on the above design principle, the titled sulfonated poly(*para*-phenylene)s, SPP-BP-CH_3 and -CF_3,

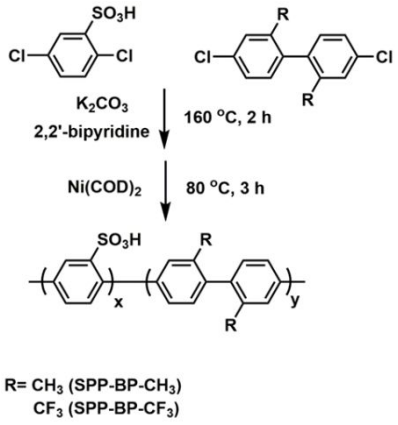

Scheme 1 Synthesis of SPP-BP-CH_3 and -CF_3 Copolymers.

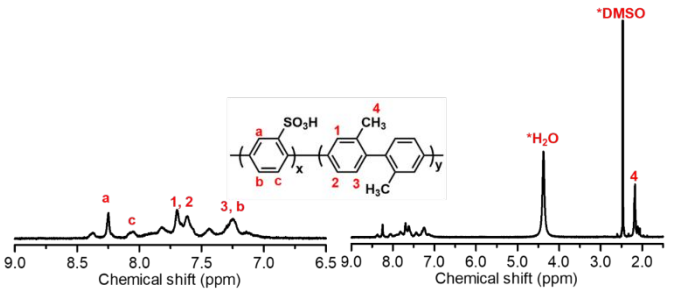

Fig. 2 ^{1}H NNR spectrum for SPP-BP-CH_3-2.9 in DMSO-d_6 at 80 °C.

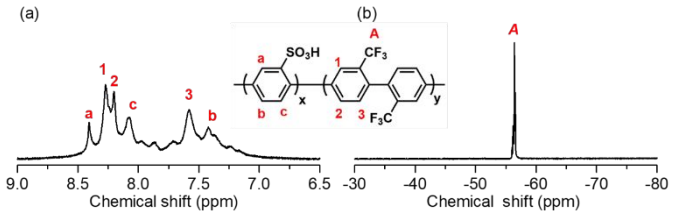

Fig. 3 (a) ^{1}H and (b) ^{19}F NNR spectra for SPP-BP-CF_3-2.7 in DMSO-d_6 at 80 °C.

Table 1 Composition, molecular weight, IEC, yield, solubility, and membrane forming capability of SPP-BP-CH_3 and -CF_3.

Polymer	Composition				M_n[c] (kDa)	M_w[c] (kDa)	IEC (mequiv. g^{-1})			Yield (%)	Solubility[d]		Membrane forming capability[e]
	x[a]	y[a]	x[b]	y[b]			Feed	NMR	Titration		DMSO	Ethanol	
SPP-BP-CH_3													
-2.2	0.80	1.00	0.69	1.00	34	102	2.6	2.4	2.2	97	B	C	×
-2.7	1.02	1.00	0.90	1.00	30	88	3.0	2.8	2.7	97	B	C	▲
-2.9	1.39	1.00	1.15	1.00	28	95	3.5	3.2	2.9	97	A	C	○
-3.3	1.92	1.00	1.69	1.00	29	100	4.0	3.8	3.3	96	A	C	○
SPP-BP-CF_3													
-2.1	1.25	1.00	1.02	1.00	101	234	2.6	2.3	2.1	96	A	A	○
-2.6	1.67	1.00	1.43	1.00	105	211	3.0	2.8	2.6	95	A	A	○
-2.7	2.22	1.00	1.85	1.00	149	316	3.5	3.2	2.7	95	A	A	○
-3.4	3.03	1.00	2.70	1.00	49	161	4.0	3.8	3.4	97	A	A	○

[a] Calculated from feed comonomer ratio. [b] Calculated from ^{1}H NMR spectra. [c] Apparent molecular weights were estimated from GPC (calibrated using polystyrene standards). [d] A, soluble; B, partially soluble; C, insoluble. [e] ×, did not form membrane; ▲, untransparent membrane; ○, transparent membrane.

were synthesized by the copolymerization of sulfonated *para*-phenylene (SP) and bis-methylated or bis-trifluoromethylated *para*-biphenylene monomers (BP-CH_3 or -CF_3, respectively) as shown in Scheme 1. The hydrophobic monomers were prepared from *m*-toluidine or 2,2'-bis(trifluoromethyl)benzidine by Sandmeyer reaction in reasonable yields (Scheme S1). The chemical structure of the hydrophobic monomers was analyzed by NMR spectra, where all peaks were well-assigned to the supposed structure (Figs. S1 and S2). The copolymerization was carried out in the presence of Ni(0) promoter. By changing the feed comonomer ratio, a series of SPP-BP-CH_3 or -CF_3 with different ion exchange capacity (IEC) were obtained in high yields (> 95%) (Table 1). SPP-BP-CH_3 copolymers showed limited solubility with IEC dependence; the SPP-BP-CH_3 with IEC ≥ 2.9 mequiv. g^{-1} were highly soluble in polar aprotic solvents such as DMSO. The SPP-BP-CF_3 copolymers were more soluble than the SPP-BP-CH_3: all SPP-BP-CF_3 were highly soluble not only in DMSO, but also in polar protic solvents such as ethanol, presumably because of the affinity of the fluorine groups with the alcohol. Smaller persistence length may also be responsible. The chemical structures of these two series of the copolymers were analyzed by ^{1}H and ^{19}F NMR spectra, where the peaks were well-assigned to the structure as shown in Figs. 2 and 3. The copolymer composition was estimated from the peak integrals in the ^{1}H NMR spectra (Table 1). At any composition, the resulting copolymers contained somewhat lower amount of the SP unit (i.e., 12-17% lower x for SPP-BP-CH_3 and 11-18% lower x for SPP-BP-CF_3, respectively) than the feed composition. The apparent molecular weights of SPP-BP-CH_3 and -CF_3 were estimated by gel permeation chromatography (GPC) as shown in Table 1. SPP-BP-CF_3 possessed higher M_n and M_w than those of SPP-BP-CH_3 of the same feed comonomer ratio probably because of higher reactivity of BP-CF_3 than that of BP-CH_3 due to the strong electron-withdrawing nature of the CF_3 substituents. Flexible and transparent membranes were obtained for SPP-BP-CH_3 and -CF_3 copolymers by solution casting except for SPP-BP-CH_3-2.2 and -2.7. As expected, poly(*para*-phenylene)s with low linearity (or low l_p value) and planarity exhibited membrane forming capability, which was provoked by the substituents. Lack of membrane forming capability for lower-IEC SPP-BP-CH_3-2.2 and -2.7 was caused by the lower solubility in the cast solvent (i.e., partially soluble in DMSO and insoluble in ethanol). The titrated IEC values of the membranes were somewhat lower than the IECs estimated by the ^{1}H NMR spectra (i.e., 4-13% lower IEC for SPP-BP-CH_3 and 7-16% lower IEC for SPP-BP-CF_3, respectively) suggesting that part of the SO_3H groups did not function as ion exchangeable groups.

Morphology

Fig. 4 displays TEM images of the SPP-BP-CH_3 and -CF_3 membranes stained with Pb^{2+} ions. While both series of the membranes showed phase-separated morphology based on hydrophilic/hydrophobic differences in the components, the domain interfaces were more distinct for SPP-BP-CF_3 membranes. The hydrophilic (dark area) and hydrophobic (bright area) domain sizes were estimated from the images (averaged for 50 spots) and are plotted as a function of IEC in Fig. 5. The hydrophilic domain size ranged from 2.5 to 3.9 nm for SPP-BP-CH_3 and 4.2 to 4.4 nm for -CF_3 membranes. The larger hydrophilic domain size for SPP-BP-CF_3 membranes might result from the stronger hydrophobicity of the CF_3 groups than that of CH_3 groups and higher molar composition of the sulfonated phenylene groups for SPP-BP-CF_3 membrane than for SPP-BP-CH_3 membrane. In contrast, the hydrophobic domain size was similar for both membranes (1.9 to 3.0 nm for SPP-BP-CH_3 and 2.2 to 3.4 nm for -CF_3 membranes). The hydrophobic domain size decreased with increasing the IEC,

probably because the molar composition of the hydrophobic monomer decreased.

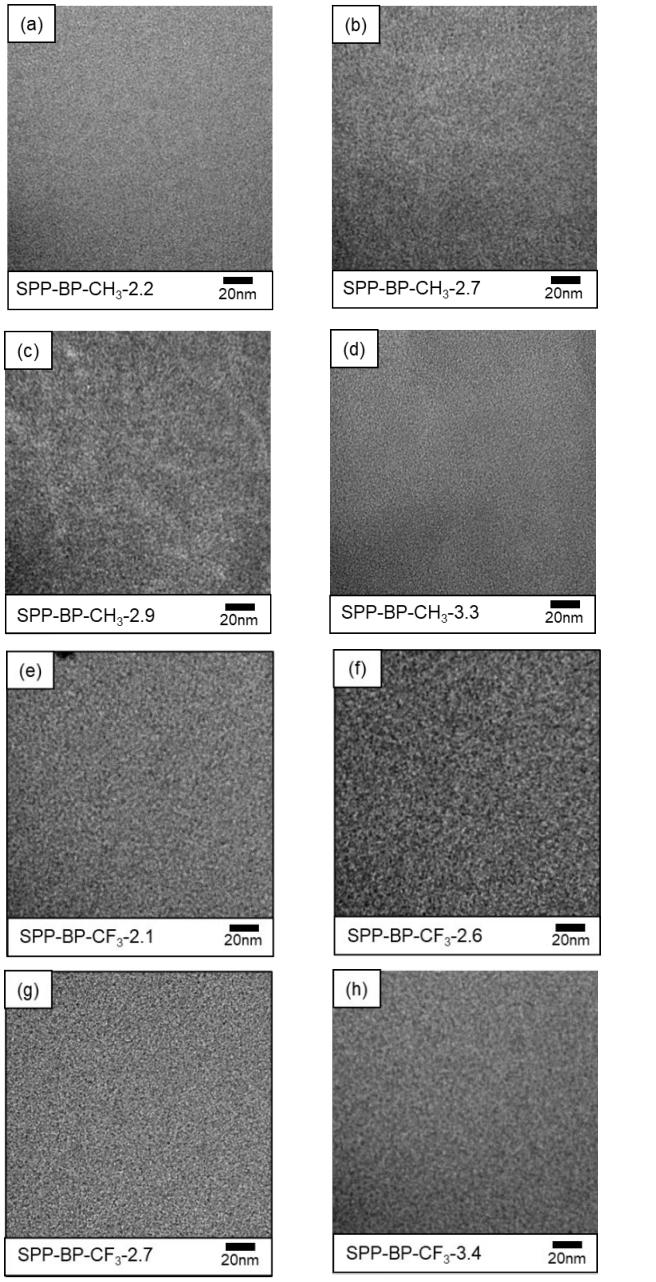

Fig. 4 TEM images of SPP-BP-CH_3 (a-d) and SPP-BP-CF_3 (e-h) membranes with different IECs stained with Pb^{2+} ions.

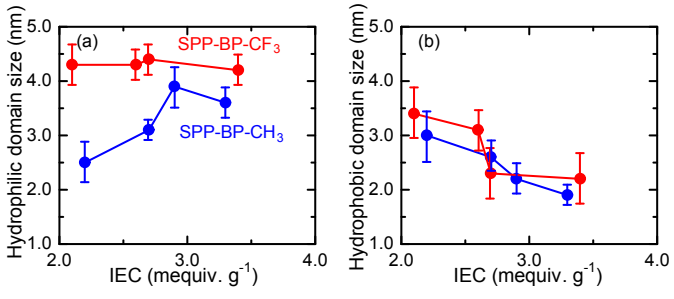

Fig. 5 (a) Hydrophilic and (b) hydrophobic domain size for Pb^{2+}-stained SPP-BP-CH_3 and -CF_3 membranes calculated from the TEM images.

Effect of water on the morphology of SPP-BP-CH_3 and -CF_3 membranes was explored by small-angle X-ray scattering (SAXS) at 80 °C and different relative humidity. Fig. S3 shows the scattered intensity as a function of the scattering vector (q). No obvious peaks were observed in all SPP-BP-CH_3 and -CF_3 membranes with different IECs at any humidity investigated, indicating that the uniform ionic clusters were not formed.[32] The periodic ionic clusters did not develop probably because of the small and rigid polymer components.[33,34] In our previous study, SPP-BAF membranes[35] containing CF_3 groups as hexafluoroisopropylidene groups in the main chain showed similar behavior. Minor difference in the electron density between the clusters and the surrounding domains would also be responsible.[36] SPP-BP-CH_3 and -CF_3 membranes showed negligible humidity dependence in SAXS profiles indicating no or minor change of the morphology upon hydration. In the background-corrected SAXS profiles (Fig. S4), the slopes in the Porod region were ca. -1.5 - -1.6, illustrating that rod and planar structures co-existed in the hydrated SPP-BP-CH_3 membranes.[37] The slopes were unavailable for SPP-BP-CF_3 membranes due to insufficient intensities with low S/N ratios in the background-corrected profiles.

Water uptake and proton conductivity

Water molecules play a crucial role in proton transport in the proton exchange membranes. The water uptake and proton conductivity of SPP-BP-CH_3 and -CF_3 membranes were measured at 80 °C and are plotted as a function of the titrated IEC in Fig. 6 (proton conductivity of the SPP-BP-CH_3 membranes with IEC = 2.2 and 2.7 mequiv. g^{-1} was unavailable due to the mechanical failure during the measurement). The water uptake increased with the increasing the humidity and IEC. At 95% RH, the water uptake increased from 32% to 53% (open circles) and 35% to 79% (closed circles) for the SPP-BP-CH_3 and -CF_3, respectively. Probably, the larger hydrophilic domain size of the SPP-BP-CF_3 membranes as suggested by TEM images was responsible. As listed in Table S1, swelling ratios of SPP-BP-CH_3 and -CF_3 membranes were lower than 12% at r.t. under fully hydrated state. The swelling was isotropic, similar swelling in in-plane and through-plane directions, implying that polymer backbone tended to arrange randomly because of the weak interchain interactions.[38] The proton conductivity also increased with increasing the IEC up to 2.7 mequiv. g^{-1} but decreased at higher IEC; the proton conductivity of the SPP-BP-CF_3 was the highest (338 mS cm^{-1} at 95% RH) for IEC = 2.7 mequiv. g^{-1} and decreased by 14% for IEC = 3.4 mequiv. g^{-1}. The proton conductivity exhibited the similar tendency at lower humidity. The increase in water uptake did not correlate with the decrease of the proton conductivity, meaning that the absorbed water did not contribute effectively to the proton conduction for higher IEC membranes. Fig. 8 represents proton diffusion coefficient (D_σ) of the membranes calculated from the Nernst-Einstein equation as a function of the volumetric IEC (IECv, mequiv. cm^{-3}). The D_σ of the membranes showed volcano-

type dependence on the IECv regardless of the CH_3 or CF_3 substituent, where the maximum D_σ shifted to smaller IECv as increasing the humidity (Fig. 7(a)). The D_σ increased with the number of water molecules per sulfonic acid group (λ) and reached plateau at λ > ca. 10 (Fig. 7(b)), probably because:1) the excess absorbed water for the higher IEC membranes diluted the concentration of sulfonic acid groups and 2) water tended to locate in the hydrophobic domains as well as in the hydrophilic ones for the higher IEC membranes.[39] Dilution of the sulfonic acid groups and water distributed in the hydrophobic domain both did not contribute much to the proton conduction.

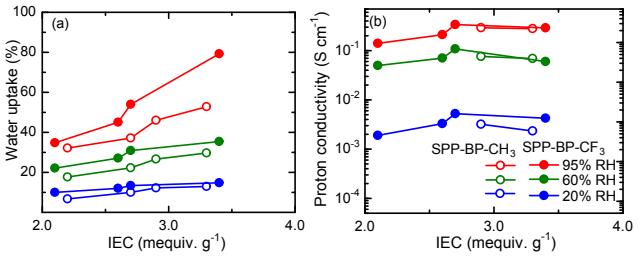

Fig. 6 IEC dependence of (a) water uptake and (b) proton conductivity of SPP-BP-CH_3 and -CF_3 at 20%, 60%, and 95% RH and 80 ℃.

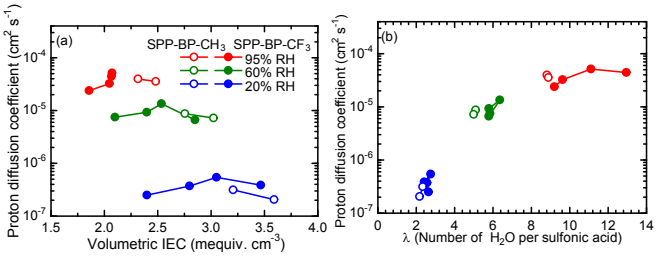

Fig. 7 Proton diffusion coefficient of SPP-BP-CH_3 and -CF_3 membranes as a function of (a) volumetric IEC (IECv) and (b) λ at 80 ℃.

Then, the water uptake and proton conductivity of SPP-BP-CH_3 and -CF_3 membranes were measured at 100 ℃ as shown in Fig. S5. For SPP-BP-CF_3 membranes, as increasing the temperature from 80 ℃ to 100 ℃, the water uptake decreased both at high (80%RH) and low (20% RH) humidity, suggesting the water affinity of SPP-BP-CF_3 membrane became smaller at higher temperature.[40] In contrast, the water uptake stayed the same or slightly increased as elevating the temperature for SPP-BP-CH_3 membranes. Nevertheless, the conductivity slightly increased as increasing the temperature for both membranes. It is known that the proton diffusion coefficient rose with the temperature,[41] and in the present case, the effect was confirmed in Fig. S5(c) and (d).

Mechanical properties

Stress versus strain curves were measured for the membranes at 80 ℃ and 60% RH (Fig. 8) and the tensile properties are summarized in Table 2. Young's modulus seemed less dependent on the substituents, l_p value, IEC, and molecular weight of the copolymers and were similar for the all membranes (Fig. S6). SPP-BP-CF_3 showed higher maximum strain (2.9-5.2%) than those (1.1-2.1%) of SPP-BP-CH_3, reflecting former's possibly lower l_p value (87.7 nm for BP-CF_3 homopolymer and 350.6 nm for BP-CH_3 homopolymer, respectively) and higher molecular weight (M_n = 49-149 kDa, M_w = 161 - 316 kDa for SPP-BP-CF_3 and M_n = 28 - 30 kDa, M_w = 88-100 kDa for SPP-BP-CH_3, respectively). Rupture energy decreased as increasing the IEC and increased as increasing the molecular weight. The higher rupture energy of SPP-BP-CF_3 membranes than that of SPP-BP-CH_3 membranes was a result of the formers' higher maximum strain.

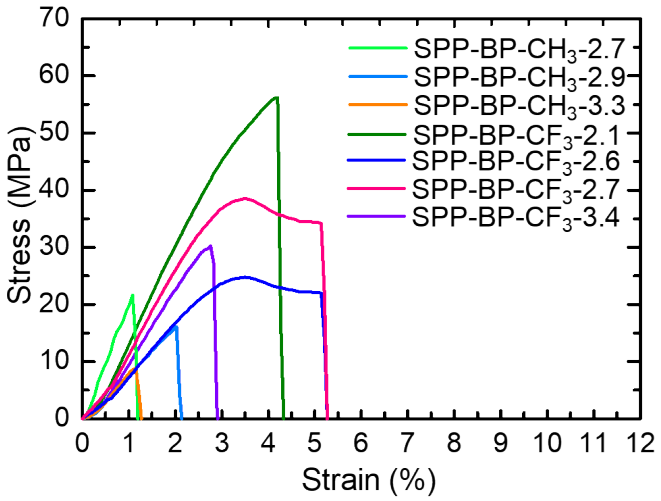

Fig. 8 Stress-strain curves of SPP-BP-CH_3 and -CF_3 at 80 ℃ and 60% RH.

Table 2 Tensile properties of SPP-BP-CH_3 and -CF_3 at 80 ℃ and 60% RH.

Membrane	Young's modulus (GPa)	Maximum stress (MPa)	Maximum strain (%)	Rupture energy (MJ m^{-3})
SPP-BP-CH_3				
2.7	2.3	21.6	1.1	0.12
2.9	0.9	16.1	2.1	0.15
3.3	1.0	8.7	1.2	0.05
SPP-BP-CF_3				
2.1	1.5	56.2	4.3	1.29
2.6	1.0	24.8	5.2	0.87
2.7	1.4	38.5	5.2	1.36
3.4	1.3	30.3	2.9	0.43

Then, viscoelastic properties (storage modulus (E'), loss modulus (E"), and tan δ (E"/E')) were evaluated at 80 ℃ as a function of the humidity (Fig. S9). For all membranes, E' decreased as increasing the humidity because the absorbed water softened the membranes. The E" and tan δ did not show

any obvious peaks indicating that these membranes did not possess glass transition under the test conditions. The E' and E" were not dependent on the substituents and IEC (Fig. S10). At ca. 80 ℃ and 0% RH, the E' (3.88-6.76 GPa) and E" (0.11-0.34 GPa) were much higher than those (E' = 2.78 GPa, E" = 0.0691 GPa) for SPP-QP (sulfonated poly(*para*-/*meta*-phenylene) with no CH_3 and CF_3 substituents),[24] probably because of the absence of the kinked *meta*-phenylene groups in the SPP-BP-CH_3 and -CF_3 backbones.

Gas permeability

Considering the balanced proton conductivity and mechanical properties, SPP-BP-CH_3-2.9 and -CF_3-2.7 membranes were selected to measure the gas permeation properties. Hydrogen and oxygen permeability of SPP-BP-CH_3, -CF_3 and Nafion-212 was measured at 80 ℃ and plotted as a function of the humidity in Fig. 9. The gas permeability increased as increasing the humidity due to the plasticization induced by water sorption.[42] It was noticed that SPP-BP-CH_3-2.9 and SPP-BP-CF_3-2.7 exhibited smaller hydrogen and oxygen permeability than that of Nafion-212 at any humidity, reflecting the intrinsic properties of aromatic polymer-based ionomer membranes.[24] Compared with SPP-BP-CH_3-2.9 membrane, the SPP-BP-CF_3-2.7 membrane showed higher gas permeability (in particular, oxygen), which was caused by higher gas (oxygen) solubility of partially fluorinated polymer membranes.[43]

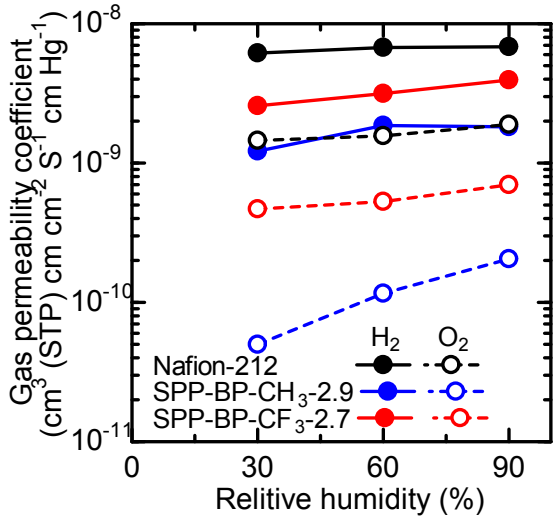

Fig. 9 Hydrogen and oxygen permeability of SPP-BP-CH_3-2.9, -CF_3-2.7 and Nafion-212 membranes at 80 ℃ as a function of the humidity.

Oxidative stability

The oxidative stability of SPP-BP-CH_3 and -CF_3 membranes was evaluated by immersing into Fenton's reagent at 80 ℃ for 1 h (Fig. 10). After the Fenton's test, all the SPP-BP-CH_3 (retaining 95~100%) and SPP-BP-CF_3 (retaining 96~100%) membranes retained the titrated IEC values (Table S2), indicating that the -SO_3H groups were intact under the harsh oxidative conditions. However, SPP-BP-CH_3 membranes lost weight (retaining 77~85%) and molecular weight (retaining 46~95%). To understand the oxidative degradation of SPP-BP-CH_3 membranes in more details, Fig. S11 compares the ^{1}H NMR spectra between before and after the Fenton's test, where methyl proton peak was smaller for the post-test samples. Furthermore, the polydispersity index (PDI) increased from 3.0 ~ 3.5 to 5.1 ~ 6.3. These results indicate that the main chain degradation occurred for SPP-BP-CH_3 probably triggered by the oxidative decomposition of the methyl groups. The lower molecular weight portion of the polymer produced by the oxidative degradation must have caused the eventual weight loss. Besides, the degradation was more significant for higher IEC polymer despite the lower content of the methyl groups because the higher IEC membrane absorbed more water to have higher chances of the oxidative attack by the hydroxyl radicals. SPP-BP-CF_3 membranes were more oxidatively stable and showed minor changes in weight, molecular weight, and ^{1}H and ^{19}F NMR spectra after the Fenton's test, similar to the poly(*meta*-/*para*-phenylene) ionomer (SPP-QP) membranes containing no substituents other than the sulfonic acid groups.[24] The results suggest that the electron-withdrawing CF_3 groups were stable and did not deteriorate the oxidative stability of the polyphenylene ionomer membranes.

The post-test SPP-BP-CH_3 membranes were fragile, while SPP-BP-CF_3 membranes remained flexible without detectable cracks

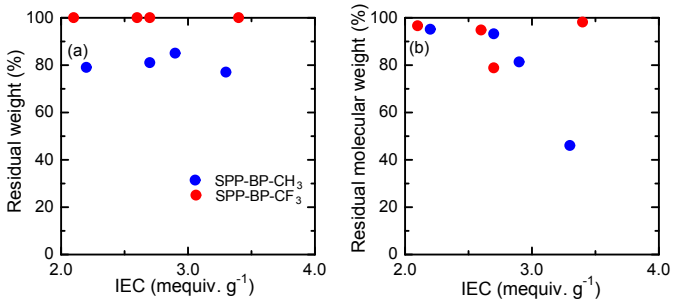

Fig. 10 IEC dependence of residual (a) weight and (b) molecular weight of SPP-BP-CH_3 and -CF_3 membranes after Fenton's test.

and pinholes which made them possible for some properties measurements. The water uptake, proton conductivity and viscoelastic properties of the post-test and pristine membranes were comparable (Figs. S12 and S13). The SPP-BP-CF_3-2.7 membrane, however, exhibited observable decrease in the conductivity since the conductivity was relatively sensitive to the minor changes in IEC around this IEC region (Fig. 6). Fig. S14 compares the stress-strain curves of the SPP-BP-CF_3 membranes between before and after the Fenton's test. The SPP-BP-CF_3-2.1 did not change in maximum stress and strain. The post-test SPP-BP-CF_3-2.6 and -2.7 membranes showed larger maximum stress and comparable maximum strain, while the post-test SPP-BP-CF_3-3.4 membrane showed smaller maximum stress and smaller maximum strain. Those differences were not very significant and might have caused by some minor changes of the conformation and/or polymer chain entanglement being taken place during the test.

Conclusions

In order to obtain high-molecular-weight, sulfonated poly(*para*-phenylene)s with solvent solubility and membrane-forming capability, effects of methyl and trifluoromethyl substituents were investigated. For the purpose, two types of monomers, 2,2'-dimethyl- (or 2,2'-bis(trifluoromethyl)-) 4,4'-dichloro biphenyl (BP-CH_3 or -CF_3) were designed and synthesized. The numerical calculation indicated that while unsubstituted poly(*para*-phenylene) possessed infinite persistence length (l_p), the l_p decreased significantly (or the polymers tended to have more bent structure) to ca. 350.6 nm for BP-CH_3 and ca. 87.7 nm for BP-CF_3, respectively. By the Ni(0)-mediated copolymerization of 1,4-dichloro-2-sulfobenzene (SP) with the above BP-CH_3 and -CF_3 monomers, two series of sulfonated poly(*para*-phenylene)s with the substituents (SPP-BP-CH_3 and -CF_3) were successfully synthesized in high yields (> 95%). Both series of the copolymers exhibited high molecular weight (M_n = 28 – 30 kDa, M_w = 88 – 100 kDa for SPP-BP-CH_3 and M_n = 49 – 149 kDa, M_w = 161 – 316 kDa for SPP-BP-CF_3, respectively) and solvent solubility. SPP-BP-CF_3 were soluble not only in DMSO but also in ethanol, whereas SPP-BP-CH_3 was only soluble in DMSO reflecting the differences in the linearity of those poly(*para*-phenylene)s; stronger interpolymer interactions were expected for SPP-BP-CH_3 with larger l_p values. Similarly, SPP-BP-CF_3 with smaller l_p values exhibited better membrane-forming capability and mechanically stability than SPP-BP-CH_3. The obtained SPP-BP-CF_3 membranes showed higher water uptake attributable to more distinct hydrophilic/hydrophobic phase-separated morphology. Furthermore, SPP-BP-CF_3 membranes survived the Fenton's test with minor changes in weight, IEC, molecular weight, and chemical structure, while SPP-BP-CH_3 membranes lost molecular weight, in particular, for higher IEC membranes. The hydrophobic, and electron-withdrawing CF_3 groups were effective in providing sulfonated poly(*para*-phenylene)s with multiple attractive properties (solvent solubility, membrane formability, high proton conductivity, mechanical strength, and chemical stability). The results suggest further possibility of poly(*para*-phenylene) derivatives as functional polymer materials by simply introducing and adjusting appropriate substituents.

Conflicts of interest

There are no conflicts to declare.

Author contributions

Fanghua Liu: Investigation, writing
Jinju Ahn: Investigation, writing
Junpei Miyake: Methodology, reviewing and editing
Kenji Miyatake: Supervision, conceptualization, writing, reviewing and editing, funding acquisition, and project administration

Acknowledgements

This work was partly supported by the New Energy and Industrial Technology Development Organization (NEDO), JSPS KAKENHI (18H05515, 21H01650), Japan Science and Technology (JST) through SICORP (JPMJSC18H8), JKA promotion funds from AUTORACE, by the thermal and electric energy technology foundation, and CHINA SCHOLARSHIP COUNCIL.

Notes and references

1 M. Remmers, B. Müller, K. Martin, H.-J. Räder and W. Köhler, *Macromolecules*, 1999, **32**, 1073–1079.
2 T. Yamamoto and A. Yamamoto, *Chem. Lett.*, 1977, **6**, 353-356.
3 P. Kovacic and M. Jones, *Chem. Rev.*, 1987, **87**, 357-379.
4 C. Le. Ninivin, A. B. Longeau, D. Demattai, P. Palmas, J. Saillard, C. Coutanceau, C. Lamy and J. M. Leger, *J. Appl. Polym. Sci.*, 2006, **101**, 944-952.
5 X. Zhang, T. Higashihara, M. Ueda and L. Wang, *Polym. Chem.*, 2014, **5**, 6121-6141.
6 Z. Qiu, B. Hammer and K. Müllen, *Prog. Polym. Sci.*, 2020, **100**, 101179.
7 T. Wallow and B. Novak, *J. Am. Chem. Soc.*, 1991, **113**, 7411-7412.
8 T. Yokozawa, H. Kohno, Y. Ohta and A. Yokoyama, *Macromolecules*, 2010, **43**, 7095–7100.
9 K. Umezawa, T. Oshima, M. Yoshizawa-Fujita, Y. Takeoka and M. Rikukawa, *ACS Macro Lett.*, 2012, **1**, 969-972.
10 A. Baun, Z. Wang, S. Morsbach, Z. Qiu and A. Narita, *Macromolecules*, 2020, **53**, 5756-5762.
11 C. Frick, A. DiRienzo, A. Hoyt, D. Safranski, M. Saed, E. Losty and C. Yakacki, *J. Biomed. Mater. Res., Part A*, 2014, **102**, 3122-3129.
12 V. Percec, M. Zhao, J. Bae and D. Hill, *Macromolecules*, 1996, **29**, 3727-3735.
13 V. Percec, J. Bae, M. Zhao and D. Hill, *Macromolecules*, 1995, **28**, 6726-6734.
14 R. Vaia, D. Dudis and J. Henes, *Polymer*, 1998, **39**, 6021-6036.
15 R. Phillips, V. Sheares, E. Samulski and J. DeSimone, *Macromolecules*, 1994, **27**, 2354-2356.
16 Y. Takeoka, K. Umezawa, T. Oshima, M. Yoshida, M. Yoshizawa-Fujita and M. Rikukawa, *Polym. Chem.*, 2014, **5**, 4132–4140.
17 C. Alegre, A. Lozano, A. Manso, L. Álvarez-Manuel, F. Marzo and F. Barrera, *Appl. Energy* 2019, **250**, 1176–1189.
18 M. Adamski, N. Peressin and S. Holdcroft, *Mater. Adv.*, 2021, **2**, 4966–5005.
19 M. Zaton, J. Roziere and D. Jones, *Sustainable Energy Fuels*, 2017, **3**, 409–438.
20 M. Adamski, T. Skalski, B. Britton, T. Peckham, L. Metzler and S. Holdcroft, *Angew. Chem.*, 2017, **129**, 9186-9189.
21 S. Ozasa, N. Hatada, Y. Fujioka and E. Ibuki, *Bull. Chem. Soc. Jpn.*, 1980, **53**, 2610-2617.
22 K. Shiino, J. Miyake and K. Miyatake, *Chem. Commun.*, 2019, **55**, 7073-7076.
23 N. Peressin, M. Adamski, E. Schibli, E. Ye, B. Frisken and S. Holdcroft. *Macromolecules*, 2020, **53**, 3119-3138.
24 J. Miyake, R. Taki, T. Mochizuki, R. Shimizu, R. Akiyama, M. Uchida and K. Miyatake, *Sci. Adv.*, 2017, **3**, eaao0476.
25 M. Litt, S. Granados-Focil, J. Kang, K. Si and R. Wycisk, *ECS Trans.*, 2010, **33**, 695–710.
26 K. Si, D. Dong, R. Wyciskc and M. Litt, *J. Mater. Chem.*, 2012, **22**, 20907-20917.
27 K. Wunderlich, K. Müllen and G. Fytas, *Mater. Energy*, 2018, 1-28.
28 B. Kuei and E. Gomez, *Soft Matter*, 2017, **13**, 49-67.

29 S. Vanhee, R. Rulkens, U. Lehmann, C. Rosenauer, M. Schulze, W. Köhler and G. Wegner, *Macromolecules*, 1996, **29**, 5136-5142.
30 W. Zhang, E. Gomez and S. Milner, *Macromolecules*, 2014, **47**, 6453-6461.
31 I. Cacelli and G. Prampolini, *J. Phys. Chem. A*, 2003, **107**, 8665-8670.
32 Y. Liu, J. Horan, G. Schlichting, B. Caire, M. Liberatore, S. Hamrock, G. Haugen, M. Yandrasits, S. Seifert and A. Herring, *Macromolecules*, 2012, **45**, 7495-7503.
33 T. Mochizuki, K. Kakinuma, M. Uchida, S. Deki, M. Watanabe and K. Miyatake, *ChemSusChem*, 2014, **7**, 729-733.
34 K. Shiino, T. Otomo, T. Yamada, H. Arima, K. Hiroi, S. Takata, J. Miyake and K. Miyatake, *ACS Appl. Polym. Mater.*, 2020, **2**, 5558-5565.
35 J. Ahn, R. Shimizu and K. Miyatake, *J. Mater. Chem. A.*, 2018, **6**, 24625-24632.
36 Y. Luan, Y. Zhang, H. Zhang, L. Li, H. Li and Y. Liu, *J. Appl. Polym. Sci.*, 2008, **107**, 396–402.
37 A. Kusoglu, M. Modestino, A. Hexemer, R. Segalman and A. Weber, *ACS Macro Lett.*, 2012, **1**, 33-36.
38 X. Zhang, Z. Hu, Y. Pu, S. Chen, J. Ling, H. Bi, S. Chen, L. Wang and K. Okamoto, *J. Power Sources*, 2012. **216**, 261-268.
39 L. He, C. Fujimoto, C. Cornelius and D. Perahia, *Macromolecules*, 2009, **42**, 7084–7090.
40 Z. Long and K. Miyatake, *ACS Appl. Mater. Interfaces*, 2021, **13**,15366-15372.
41 Z. Taherkhani, A. Mahdi and S. Alireza, *J. Electrochem. Soc.*, 2015, **162**, F1096-F1100.
42 S. Simon, E. Espuche, F. Gouanv´e, E. Chauveau, C. Marestin and R. Mercier, *J. Phys. Chem. B*, 2012, **116**, 12750-12759.
43 Y. Zhang, J. Miyake, R. Akiyama, R. Shimizu and K. Miyatake, *ACS Appl. Energy Mater.* 2018, **1**, 1008-1015.